Editors' Suggestion

Photonic Heterostructures for Spin-Flipped Beam Splitting

Chuanning Niu,[1] Zuojia Wang,[1,*] Jia Zhao,[1] Liuge Du,[1] Na Liu,[1] Yongmin Liu,[2] and Xun Li[1,3]

[1] *School of Information Science and Engineering, Shandong University, Qingdao 266237, China*

[2] *Department of Mechanical and Industrial Engineering, Department of Electrical and Computer Engineering, Northeastern University, Boston, Massachusetts 02115, USA*

[3] *Department of Electrical and Computer Engineering, McMaster University, Hamilton, Ontario L8S 4K2, Canada*

(Received 9 May 2019; revised manuscript received 19 August 2019; published 4 October 2019)

Understanding and controlling chirality are important because of its ubiquity in nature. In recent years, we have witnessed the rapid development of chiral metamaterials with exceptional light-manipulating capabilities. Here, we present a design for photonic heterostructures in chiral photonics, demonstrating that photonic heterostructures stacked from achiral metasurfaces can create distinctive chiroptical functionalities. Analyses based on the symmetry group and microscopic dipolar interactions at two-dimensional boundaries reveal the implicit mechanism of the interlayer coupling in photonic heterostructures. By flip stacking, the photonic heterostructure gives rise to an asymmetric chiral phase from achiral composites, and hence, provides the full spin-flipped scattering of incident photons. Incident electromagnetic waves with arbitrary polarization orientations can be efficiently separated into two orthogonal circularly polarized ones with orthogonal trajectories, leading to an ideal circular beam splitter. This effect is experimentally demonstrated at microwave frequencies via the measurement of a scattering matrix. Due to its generality and scalability, we expect the methodology of photonic heterostructure might open up an alternative pathway for exploring intriguing and advanced metamaterials over a broad wavelength range.

DOI: 10.1103/PhysRevApplied.12.044009

I. INTRODUCTION

An object is chiral if it cannot be superimposed on its mirror image by translational and rotational transformations. Chirality is a ubiquitous geometric property in our natural life, ranging from macrostructures, such as human hands, to microstructures, such as molecules [1,2]. Chiral interactions are known to affect the electron transmission [3,4], optical responses [5], and magnetic skyrmions [6,7] in materials; pharmacological effects in drugs [8,9]; and other nontrivial phenomena in various disciplines. Due to profound implications for various disciplines, the study and manipulation of chiral interactions have attracted continuing interest from scientists. In particular, chiral optics studies the behavior of circularly polarized light when it interacts with chiral media. The chiroptical effects in naturally occurring materials are often very weak due to the size mismatch between molecules and the wavelength of light.

Metamaterials comprising arrays of designer metaatoms have been developed to achieve chiroptical responses several orders of magnitude greater than those of the natural materials [10–13]. Initial studies focused on the design of three-dimensional (3D) building blocks with intrinsic chirality. 3D helical metamaterials are fabricated by direct laser writing [14], glancing-angle deposition [15], tomographic rotatory growth [16], and self-assembly methods [17,18]. Giant circular dichroism can be achieved in such bulky metamaterials from microwave to visible frequencies [10]. Another approach is stacking and twisting achiral constituents, such as split-ring resonators [19], rods [20], arcs [21], ellipses [22], plasmonic diastereomers [23], and Moiré patterns [24], to form a 3D superstructure that is chiral. Although the concept is simple, the 3D chiral structures are highly sensitive to a number of degrees of freedom, including the twisting angle and spacing distance [11]. As the structure twists to form an intrinsic chirality, the optical response is accordingly fixed with a certain handedness [25]. In addition, the complexities in 3D fabrication and the lack of suitable low-loss materials at optical wavelengths have, so far, limited practical applications.

Metasurfaces, which are the two-dimensional (2D) counterparts to bulk metamaterials, have emerged as an alternative platform to overcome these challenges and provide giant chiral light-matter interactions [26–29]. Various chiral metasurfaces with 2D chirality have been investigated, including conjugated gammadions [30–32], shuriken-shaped indentations [33], L-shaped nanoantennas [34], and many other structures [35]. Unfortunately, a planar chiral metasurface itself does not manifest optical

*z.wang@sdu.edu.cn

activity, owing to mirror symmetry and reciprocity [36,37]. The reported optical activity in 2D planar nanostructures originates from broken symmetry at the air-structure-substrate interfaces [31]. Metasurfaces with extrinsic chirality have been demonstrated as a solution for strong 2D chiroptical effects, in which the oblique incident waves, together with the 2D metasurface, form a 3D configuration that lacks mirror symmetry [38,39]. However, the extrinsic chirality is also limited by reciprocity, and therefore, no giant circular conversion dichroism can be reached in 2D metasurfaces with an infinitesimal thickness. As a result, one of the main issues, so far, is the lack of an efficient methodology for chiral building blocks with improved efficiency, versatile functionality, and reduced complexity.

Here, we report on the design of photonic heterostructures in chiral photonics, showing how the stacking of individual 2D metasurfaces can create chiroptical functionalities that are not accessible in monolayer 2D metasurfaces. Symmetry consideration and reciprocity theorem are employed together to reveal the design principle of spin-flipped beam splitting. With suitably stacked metasurfaces, all incident photons can be separated into two orthogonal trajectories with flipped spin states, indicating an ideal prismlike chiral beam splitter. The underlying mechanism and interlayer coupling between photonic monolayers are revealed by exploring the microscopic dipolar interactions. We note that our approach is conceptually different from previous techniques aimed at engineering complicated metaatoms with intrinsic chirality, since the photonic heterostructure enables promising chirality functionalities from a much simpler design methodology. We expect that the concept of photonic heterostructure can revolutionize the methodology in the area of photonic metamaterials and metadevices.

In addition to eliminating the need for bulky and sophisticated 3D structures, the photonic heterostructure has unique physical properties that make it useful for chiral photonics. First, its chirality behavior is determined by flip stacking, rather than the twisting that is widely used in traditional approaches. Two stacking strategies, direct stacking and flip stacking, give rise to entirely distinct chiral phases. In contrast to a conventional chiral metamaterial, the photonic heterostructure is inherently achiral, but provides more chiral properties within a thin optical interface. Second, due to the stacking configuration, the photonic heterostructure is no longer subject to the theoretical limit of circular conversion efficiency at a 2D electromagnetic boundary. The spin-stacked heterostructure can realize a near-unity efficiency of circular beam splitting, along with the full spin flipping in both reflection and transmission. These features make it a good candidate for a circular beam splitter without destroying the energy balance between two spin photons upon scattering. Third, the photonic heterostructure platform exhibits useful properties for multichirality wave steering, such as asymmetric transmission and chirality switching for spin photons with opposite longitudinal and transverse momenta, respectively. It is hence suitable for optical systems in which the backward signals reflected from objects need to be suppressed, especially in chiral devices.

II. RESULTS

A. Principle of photonic heterostructure design

The design concept of photonic heterostructure and its chiroptical behavior are schematically presented in Fig. 1(a). 3D metamaterials with intrinsic chirality transmit specific circularly polarized waves (e.g., RCP waves). Due to the homogeneous chirality that is enabled by the fourfold rotational symmetry, two circular polarizations have identical characteristic impedances, and thus, LCP waves will be totally absorbed. This is the circular dichroism in normal chiral media. We call it zero spin flipping because no cross-polarized photons are generated. In 2D metasurfaces, the intrinsic chirality no longer exists due to inherent mirror symmetry with respect to the transverse plane. Only extrinsic chirality can be implemented when circularly polarized light is obliquely incident on an anisotropic structure (e.g., split-ring resonators). In this situation, a thin metasurface supports only surface electric currents and cannot efficiently absorb all incident waves. Therefore, to achieve strong chirality, one of two circular polarizations (e.g., LCP) must be reflected with its spin state flipped, while the other circular polarization (e.g., RCP) is transmitted with its spin state preserved. This is the case we called half spin flipping. To break the theoretical limit of 50% efficiency in single 2D metasurfaces, we introduce the concept of photonic heterostructure. The photonic heterostructure stacked from two identical 2D metasurfaces is proposed to fully flip the spin angular momenta of the incident photons, and simultaneously separate the two circular polarizations along two orthogonal trajectories. In other words, the photonic heterostructure behaves as an ordinary metallic mirror and a half-wave plate for LCP and RCP waves, respectively.

The underlying mechanism of the photonic heterostructure (designed for RCP waves) is depicted in Fig. 1(b). In general, upon illumination, a thin planar layer with uniformly arranged scatters is polarized both electrically and magnetically, yielding to the boundary discontinuities [40]

$$\mathbf{E}_t^{>} \times \hat{z} - \mathbf{E}_t^{<} \times \hat{z} = -i\omega \mathbf{M}_{\mathrm{TE}}, \tag{1}$$

$$\hat{z} \times \mathbf{H}_t^{>} - \hat{z} \times \mathbf{H}_t^{<} = -i\omega \mathbf{P}_{\mathrm{TE}}, \tag{2}$$

where $\mathbf{M}_{\mathrm{TE}} = \mathbf{M}_t - \hat{z} \times (\mathbf{k}_t/\omega\varepsilon)P_z$ and $\mathbf{P}_{\mathrm{TE}} = \mathbf{P}_t + \hat{z} \times (\mathbf{k}_t/\omega\mu)M_z$ represent the total equivalent tangential magnetic and electric surface polarization densities, respectively. Here, ε and μ are the permittivity and permeability of the surrounding medium, respectively; $\hat{\mathbf{z}}$ is the unit normal vector to the metasurface plane; and $\mathbf{k}_t$ is the

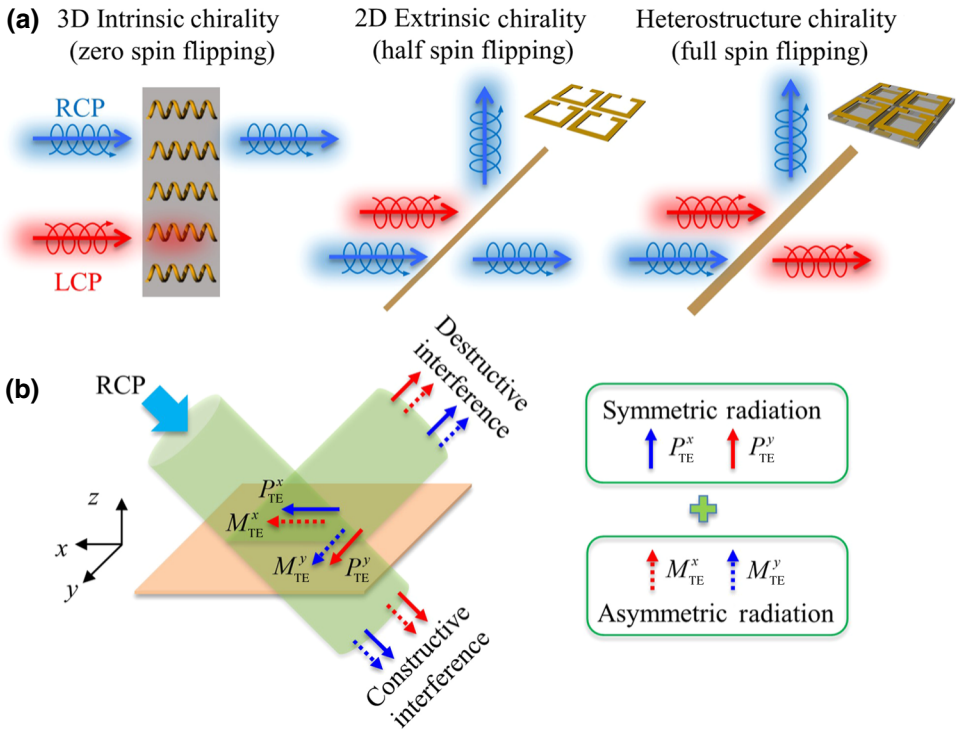

FIG. 1. Design concept and chiroptical response of the photonic heterostructure. (a) Schematic illustration of reflection and transmission by a 3D chiral metamaterial, a 2D metasurface, and a photonic heterostructure. The 3D chiral metamaterial with intrinsic chirality transmits right-handed circularly polarized (RCP) waves without flipping the spin state and absorbs all left-handed circularly polarized (LCP) waves. The 2D metasurface with extrinsic chirality reflects LCP waves back and flips the spin, which transmits RCP waves with preserved spin. The photonic heterostructure splits and flips both circularly polarized waves simultaneously. (b) The design principle for highly efficient spin-flipped transmission for RCP illumination. The induced tangential electrical and magnetic polarizations can be decomposed into right-handed and left-handed components that radiate two circular polarized waves. The symmetric and asymmetric radiation features of electrical and magnetic dipoles contribute to the directional radiation. Full spin-flipped splitting arises when radiated waves interfere destructively and constructively in reflection and transmission, respectively; this results in zero reflection.

transverse wave vector. We mark the normal and tangential components by subscripts "z" and "t", respectively. The $>$ and $<$ superscripts refer to the fields at $z = 0^+$ and 0^-, respectively. The tangential radiated fields from the surface polarizations are expressed by

$$\mathbf{E}^{>}_{t,\mathrm{rad}} = \frac{i\omega}{2}\overline{\overline{Z}} \cdot \left[\mathbf{P}_{\mathrm{TE}} - \overline{\overline{Z}}^{-1} \cdot \hat{z} \times \mathbf{M}_{\mathrm{TE}}\right], \tag{3}$$

$$\mathbf{E}^{<}_{t,\mathrm{rad}} = \frac{i\omega}{2}\overline{\overline{Z}} \cdot \left[\mathbf{P}_{\mathrm{TE}} + \overline{\overline{Z}}^{-1} \cdot \hat{z} \times \mathbf{M}_{\mathrm{TE}}\right], \tag{4}$$

with a 2×2 dyadic

$$\overline{\overline{Z}} = \eta\left(\cos\theta \frac{\mathbf{k}_t\mathbf{k}_t}{k_t^2} + \frac{1}{\cos\theta}\frac{\hat{z} \times \mathbf{k}_t\hat{z} \times \mathbf{k}_t}{k_t^2}\right),$$

where $\eta = \sqrt{\mu/\varepsilon}$ is the intrinsic wave impedance in the host medium and θ is the angle of incidence. At the two sides of the thin layer, the radiated fields of electric surface polarizations are identical in both amplitude and phase, while those of magnetic ones show 180° phase differences. In other words, electric and magnetic surfaces polarizations can generate symmetric and asymmetric radiations, respectively.

To ensure zero reflection and total spin flipping in transmission for RCP waves, the heterostructure must create a copolarized forward plane wave, which cancels the incident plane wave, and a cross-polarized forward plane wave with an equal intensity. At the same time, the heterostructure should not create any radiation in the direction towards the source. In fact, conduction or polarization currents are induced on a surface sheet by the incident waves, which radiate symmetrically in both directions, resulting in the theoretical limit of 50% efficiency for an infinitely thin absorber [41]. Therefore, magnetic surface polarization is crucial to provide asymmetric radiation and suppress the reflection channel, so as to improve the efficiency of spin flipping in transmission. Moreover, to achieve unity efficiency of spin flipping, the induced surface polarizations should radiate both LCP and RCP waves with equal

amplitudes. The radiated RCP wave then destructively interferes with the incidence and leaves only the transmission of spin-flipped photons. Such a configuration can only be realized in a stacking system consisting of at least two photonic monolayers. More detailed analysis on the surface polarizations can be found in Appendix A. Based on the above discussion, the required surface polarizations yield the following relationships:

$$M^x_{\mathrm{TE}} = \eta P^y_{\mathrm{TE}} \frac{1}{\cos\theta},\ M^y_{\mathrm{TE}} = -\eta P^x_{\mathrm{TE}} \cos\theta,\ \frac{P^x_{\mathrm{TE}}}{P^y_{\mathrm{TE}}} = \left(\frac{P^x_{\mathrm{TE}}}{P^y_{\mathrm{TE}}}\right)^*,\ \frac{M^x_{\mathrm{TE}}}{M^y_{\mathrm{TE}}} = \left(\frac{M^x_{\mathrm{TE}}}{M^y_{\mathrm{TE}}}\right)^*. \tag{5}$$

Analysis of reciprocity and symmetry group offers a theoretical tool to understand the interlayer coupling and photonically bonding mechanism in heterostructures. We consider a planar device enclosed by a fictitious boundary surface Ω around it [Fig. 2(a)]. The device inside Ω is assumed to be linear, time-dependent, and reciprocal. There are four lossless reciprocal ports for waves entering Ω, with each port comprising two orthogonal modes. For simplicity, two linear polarizations are taken into consideration. The local coordinates of each port are defined as u, v, and w, with w pointing in the forward direction (that is, into the structure). Input and output waves are described by the complex amplitudes $\vec{a}_i = [a_{iu}, a_{iv}]^T$ and $\vec{b}_i = [b_{iu}, b_{iv}]^T$, respectively. For such a linear and reciprocal system, the relation between incoming and outgoing waves can be described by a symmetric scattering matrix [36,42]:

$$\begin{bmatrix} \vec{b}_1 \\ \vec{b}_2 \\ \vec{b}_3 \\ \vec{b}_4 \end{bmatrix} = \begin{bmatrix} \mathbf{S}_{11} & \mathbf{S}_{12} & \mathbf{S}_{13} & \mathbf{S}_{14} \\ \mathbf{S}^T_{12} & \mathbf{S}_{22} & \mathbf{S}_{23} & \mathbf{S}_{24} \\ \mathbf{S}^T_{13} & \mathbf{S}^T_{23} & \mathbf{S}_{33} & \mathbf{S}_{34} \\ \mathbf{S}^T_{14} & \mathbf{S}^T_{24} & \mathbf{S}^T_{34} & \mathbf{S}_{44} \end{bmatrix} \begin{bmatrix} \vec{a}_1 \\ \vec{a}_2 \\ \vec{a}_3 \\ \vec{a}_4 \end{bmatrix}, \tag{6}$$

where $\mathbf{S}_{mn}$ is 2×2 matrix that describes how the incident wave of $\vec{a}_n$ scatters into $\vec{b}_m$. Specifically, $\mathbf{S}_{nm} = \mathbf{S}^T_{mn}$ indicates that the backward transmission matrix equals the transpose of the forward one. If the matrix is converted into the circular base, we can also relate the forward and backward circular transmission matrices for an arbitrary combination of two ports (see Appendix A)

$$\mathbf{S}^f_{\mathrm{circ}} = \begin{bmatrix} t_{\mathrm{RR}} & t^f_{\mathrm{RL}} \\ t^f_{\mathrm{LR}} & t_{\mathrm{LL}} \end{bmatrix} = (\mathbf{S}^b_{\mathrm{circ}})^T = \begin{bmatrix} t_{\mathrm{RR}} & t^b_{\mathrm{LR}} \\ t^b_{\mathrm{RL}} & t_{\mathrm{LL}} \end{bmatrix}, \tag{7}$$

with the superscripts f and b representing the forward and backward elements, respectively. Due to the reciprocity, it is clear that the spin-flipping efficiency (namely, cross-polarization transmission) yields the relations $t^f_{\mathrm{RL}} = t^b_{\mathrm{LR}}$ and $t^f_{\mathrm{LR}} = t^b_{\mathrm{RL}}$.

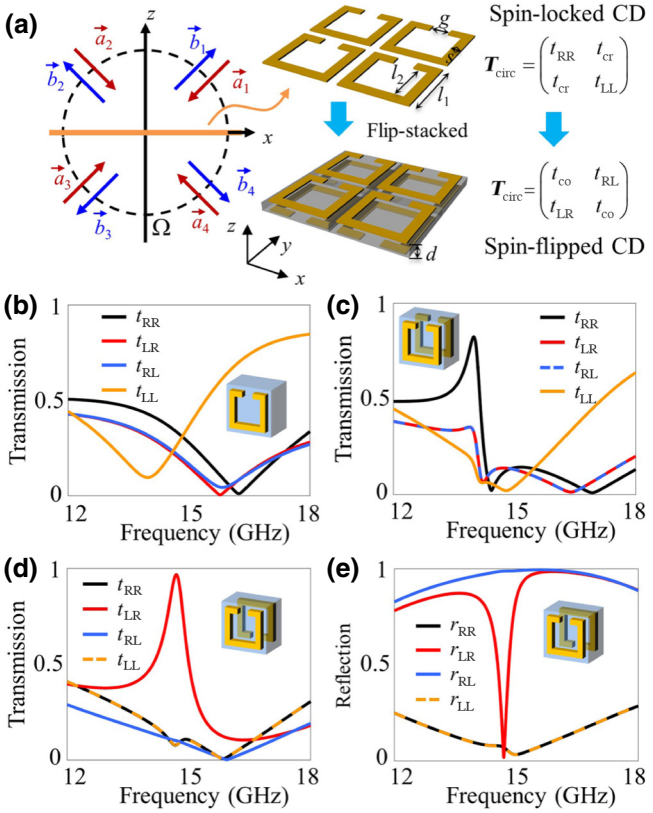

FIG. 2. The designer photonic heterostructure. (a) Transmission matrix properties of the heterostructure from flip stacking. After stacking, the macroscopic chiral phase undergoes a transition from a phase of spin-locked circular dichroism (CD) to a phase of spin-flipped CD. (b)–(d) Simulated transmission spectra for (b) single metasurface, (c) directly stacked metasurface, and (d) flip-stacked heterostructure. (e) Simulated reflection spectra of the flip-stacked heterostructure.

The symmetric group of metaatoms, along with the stacking approach, plays a critical role in the macroscopic behavior of the photonic heterostructure. Before stacking, the monolayer metasurface shown in Fig. 2(a) consists of an array of bianisotropic split-ring resonators. Due to its mirror symmetry with respect to the xy planes (M_{xy}), the circular scattering matrices have the relationships $t_{\mathrm{RL},31} = t_{\mathrm{LR},24}$ and $t_{\mathrm{LR},31} = t_{\mathrm{RL},24}$, where the subscripts "31" and "24" represent the scattering from ports 1 to 3 and 4 to 2, respectively. In addition, the structure also shows a mirror symmetry about the yz plane and thereafter the cross-polarization scattering items from port 3 to port 1 are $t_{\mathrm{RL},13} = t_{\mathrm{LR},24}$ and $t_{\mathrm{LR},13} = t_{\mathrm{RL},24}$. Subsequently, forward and backward cross-polarization transmission coefficients yield $t_{\mathrm{RL},31} = t_{\mathrm{RL},13}$ and $t_{\mathrm{LR},31} = t_{\mathrm{LR},31}$. In other words, the spin-flipping behavior obeys the relationship of $t^f_{\mathrm{LR}} = t^b_{\mathrm{RL}} = t^b_{\mathrm{LR}} = t^f_{\mathrm{RL}} = t_{\mathrm{cr}}$. For direct stacking of the photonic monolayers, such mirror symmetry is preserved, and thus, the characteristic of the scattering matrix is identical to that of a single layer. The situation becomes

completely different for the case of flip stacking. During flip stacking, the M_{xy} symmetry is broken and an additional twofold rotational symmetry, with respect to the x axis, appears. Moreover, the mirror image of the photonic heterostructure about the xz plane, from the point view of the forward direction, is identical to the photonic heterostructure itself from the point view of the backward direction. As a consequence, two copolarized transmission coefficients have identical amplitude, namely, $t_{RR} = t_{LL} = t_{co}$. This approach enables us to achieve a transition from a chiral phase of spin-locked CD to that of a spin-flipped CD.

B. The designer photonic heterostructure

According to the above design principle for stacked heterostructures, a proof-of-concept heterostructure is designed at the microwave region. As illustrated in Fig. 2(b), the single-layer metasurface with M_{xy} symmetry comprises an array of split-ring resonators with the periodicities $p_x = p_y = 8$ mm, which are much smaller than the operating wavelength to avoid undesired diffractions. The inner and outer lengths of the resonators are $l_1 = 7$ mm and $l_2 = 5$ mm, respectively, that is, the width of the arm is $s = 1$ mm. The gap size is $g = 2$ mm. Copper is selected as the material with an electric conductivity $\sigma = 5.8 \times 10^7$ S/m and a thicknesses of 0.035 mm. Figure 2(b) presents the response of the single-layer metasurface on a substrate under an oblique incident angle of $\theta = 45°$. Due to the M_{xy} symmetry of the metasurface, the cross-polarized transmission coefficients (t_{LR}, t_{RL}) for both RCP and LCP illumination are almost equal. The slight difference around 15.8 GHz is caused by the presence of the substrate. It breaks specific inversion and mirror symmetries; thus generating additional polarization effects in chirality [43]. The difference between the copolarized transmission coefficients contributes to the spin-locked CD. In the case of direct stacking [Fig. 2(c)], a chiral resonant mode is induced around 14 GHz, whereby the CD response is largely enhanced. This is the typical feature of extrinsic chirality. The simulation result of the photonic heterostructure from flip stacking is demonstrated in Figs. 2(d) and 2(e). An unprecedented photonic behavior of spin-flipped splitting happens. At 14.7 GHz, t_{LR} reaches as high as 0.97 and other transmission coefficients are less than 0.1. For comparison, r_{RL} is about 0.99, and other reflection coefficients are significantly reduced. Reflective and transmissive CDs reach 0.98 and 0.92 at this chiral resonant mode. Consequently, right-handed photons pass through the heterostructure, while the left-handed ones are totally reflected, with all of their spin angular momenta flipped. Here, F_4BM is adopted as the dielectric spacer between top and bottom metallic layers, with a relative permittivity of 2.55 and a loss tangent of 0.0015; the substrate thickness is $d = 1$ mm. More details of the performance dependence on the heterostructure geometries and angle of incidence can be found in Appendix B. It is worth mentioning that the chirality will disappear due to the existence of mirror symmetry, if the incident plane is switched to the yz plane. The proposed structure is an extension of 2D chiral asymmetry into heterostructures [38,44]. During stacking, the in-plane mirror symmetry of 2D metasurfaces can be broken and results in distinctive extrinsic chirality performance.

The discussed chiroptical effect goes beyond that of usual circular dichroism in chiral metamaterials. To validate this intriguing behavior, we fabricate a sample and perform a set of experiments with a three-port system [Fig. 3(a)]. The heterostructure is prepared by stacking two single-layer metasurfaces with a dielectric spacer between them. The bottom layer is rotated 180° about the z axis, to implement the configuration of flip stacking. A photograph of the fabricated sample is shown in Fig. 3(a) and its overall area is 200×200 mm^2. The parameters for linear polarization are measured by using a Keysight PNA-X vector network analyzer with three linear horn antennas. The reflection and transmission matrices for circular polarization are calculated from the results of linear ones. The angle of incidence is 45°, so that the propagating direction of the reflected wave is perpendicular to those of both the incident and transmitted waves. From the measured spectra in Figs. 3(b) and 3(c), we observe that the cross-polarized transmission, t_{LR}, for the RCP wave is nearly 0.88 at a resonant frequency of 14.68 GHz, while other components are very low. In the case of LCP illumination, for comparison, the incoming wave is efficiently reflected to the RCP state, with a reflection coefficient of $r_{RL} = 0.90$. As we can see, nearly perfect chiral beam splitting is realized.

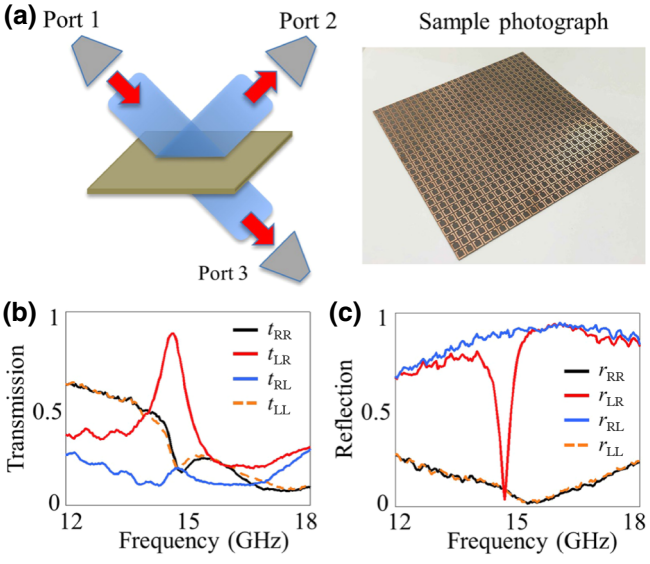

FIG. 3. Experimental measurements. (a) Schematic illustration of the measurement setup and photograph of the fabricated sample. (b) The measured transmission matrix. (c) The measured reflection matrix.

Importantly, all experiment results are in good agreement with the full-wave simulations. The slight disagreement may be caused by the fabrication precision and inaccuracy of material parameters.

C. Microscopic dipolar interactions

To better understand the underlying mechanism, we further investigate the microscopic electromagnetic response of the photonic heterostructure. As shown in Fig. 4, the E_z field distributions are plotted at two planes near the inner boundaries of the split-ring resonators. Two planes are selected: plane 1 refers to the xy plane 0.01 mm below the top resonator; plane 2 refers to the plane 0.01 mm above the bottom resonator. The surface charge distribution can be calculated from the boundary condition of the metallic surface: $\rho_{1,2} = \hat{n} \cdot \vec{D}$. The normal electric field fluxing out of the surface represents the accumulation of positive charges and *vice versa*. The patterns of surface charge density are obtained under RCP illuminations. In the case of direct stacking [Fig. 4(a)], a chiral resonance occurs at 14 GHz [the black curve in Fig. 2(c)]. As the time increases over half of a period ($T/2 = 35.7$ ps), the charge density oscillates on each resonator and creates an asymmetric quadruple mode. Two resonant modes produce out-of-plane magnetic dipoles with the same amplitude and a 180° phase difference. Moreover, the electric charge densities on the two planes exhibit intriguing symmetric properties: $\rho_1(x,y) \approx -\rho_1(-x,y)$ and $\rho_1(x,y) \approx -\rho_2(x,y)$. Consequently, the interlayer coupling between two photonic monolayers only creates strong macroscopic dipolar resonances p_y and m_y. As discussed previously, these equivalent tangential polarizations cannot produce needed radiation for the chiroptical behavior of fully spin-flipped splitting. Once the two monolayers of the heterostructure are flip-stacked, their interlayer coupling manifests distinctive responses. As shown in Fig. 4(b), the symmetric properties of the charge density distributions are destroyed, and generic electric and magnetic dipoles with all components ($\mathbf{p} = [p_x, p_y, p_z]$ and $\mathbf{m} = [m_x, m_y, m_z]$) are efficiently induced. This is the necessary condition for the desired chiroptical response, that is, simultaneous generation of tangential surface polarizations described in Eq. (5). Consequently, the photonic heterostructure flips the spin angular momenta of the incident photons and separates two circular polarizations into orthogonally propagating directions. The microscopic dipolar response contributes to the macroscopic reciprocal magnetoelectric coupling or electromagnetic chirality described by a chiral tensor $\overline{\overline{\kappa}}$ in the constitutive relations $\mathbf{D} = \overline{\overline{\varepsilon}}\mathbf{E} - (i/c)\overline{\overline{\kappa}}^T\mathbf{H}$ and $\mathrm{B} = \overline{\overline{\mu}}\mathbf{H} + (i/c)\overline{\overline{\kappa}}\mathbf{E}$ [45,46].

D. Polarization insensitivity of the chiral beam splitter

It is worth mentioning that this designer chiral beam splitter is insensitive to the polarization of the incidence. In other words, it can divide an incident wave of arbitrarily linear polarization into two orthogonally circular polarizations. To characterize this feature, we further investigate the polarization states of the transmitted and reflected waves. As shown in Fig. 5(a), the incident, reflection, and transmitted electric fields are expressed as $\mathbf{E}_i = \hat{u}_1 E_{u1} + \hat{v}_1 E_{v1}$, $\mathbf{E}_r = \hat{u}_2 E_{u2} + \hat{v}_2 E_{v2}$, and $\mathbf{E}_t =$

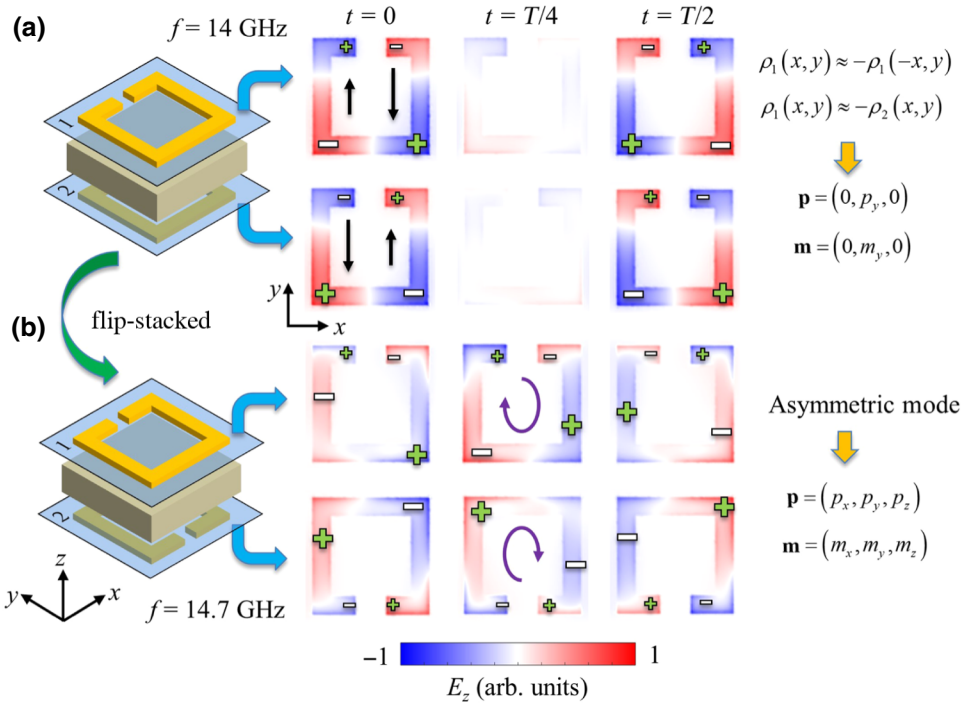

FIG. 4. Microscopic dipolar responses of the photonic heterostructure. (a) The time-dependent E_z field distributions of the directly stacked metasurface. The charge distributions indicate a symmetric resonant mode, with approximately equivalent dipolar moments of $\mathbf{p} = [0, p_y, 0]$ and $\mathbf{m} = [0, m_y, 0]$. (b) The time-dependent E_z field distributions of the flip-stacked heterostructure. An asymmetric resonant mode appears with equivalent dipolar moments of $\mathbf{p} = [p_x, p_y, p_z]$ and $\mathbf{m} = [m_x, m_y, m_z]$.

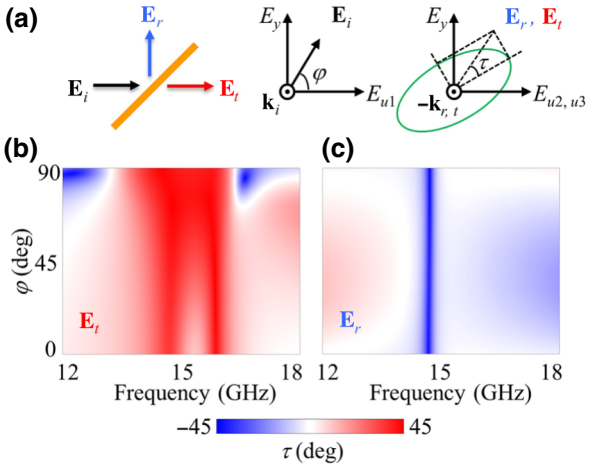

FIG. 5. Polarization insensitivity of the chiral beam splitter. (a) Schematic illustration of the defined polarization angle, φ, of the incident waves and the ellipticity angle, τ, for reflected and transmitted waves. (b),(c) The dependence of transmitted and reflected ellipticity angles on the incident polarization orientation at different frequencies.

$\hat{u}_3 E_{u3} + \hat{v}_3 E_{v3}$, respectively. The angle φ is the polarization angle of the incident wave relative to the horizontal direction in the incident plane. The ellipticity angle, τ, of the scattered electric field can be calculated by Stokes parameters [47]. Figures 5(b) and 5(c) show the dependence of the ellipticity angles of the transmitted and reflected waves on the polarization angle of the incident wave. Intriguingly, the ellipticity angle, τ, of the transmitted wave ranges from 34.7° to 43.8° at the resonant frequency of 14.7 GHz. Upon reflection, τ varies between −42.8° and −39.1° as the polarization angle φ increases. It is highly consistent with the prediction that incoming photons are equally converted into two orthogonal circular polarizations, namely, LCP in transmission and RCP in reflection channels. Such a performance is close to the behavior of a polarization-independent chiral beam splitter, which is not available in traditional circular beam splitters due to the lack of chiral eigenstates. Furthermore, compared with the circular beam splitter based on Huygens metasurfaces [48–50], the proposed mechanism does not introduce additional momenta to the incident photons and, thereafter, avoids the deflection of the photon trajectories. Specifically, another peak of the transmitted ellipticity angle, τ, rises up at 15.9 GHz, in which three transmission coefficients (t_{RL}, t_{RR}, and t_{LL}) approach zero. In this case, the transmitted energy is extremely low, and hence, it is not an efficient working frequency.

E. Asymmetric transmission and multichirality applications

Another distinctive feature of the photonic heterostructure is asymmetric transmission [51–53], that is, one designated circular polarized wave experiences different impedance when it impinges on the slab in opposite directions ($t_{RL} \neq t_{LR}$). Due to this property, interesting applications can be realized with this heterostructure. One possibility is a transverse beam splitter [Fig. 6(a)], in which the transmitted LCP waves are reflected by an ordinary reflective mirror. The spin state is thus flipped and RCP waves come back to hit the photonic heterostructure. Subsequently, the RCP waves will be reflected again in the back side of the slab. As a result, the incident waves can be divided into two orthogonal circular beams, with their propagating directions opposite to each other. Another interesting application is the chiral retroreflector, as shown in Fig. 6(b). While replacing the mirror with a polarized one, the functionality of which preserve the spin states upon reflection [54], the reflected waves will pass through the slab again and make the whole system behave as a spin-selective retroreflector. Only RCP photons can be reflected back to the time-reversed and normal trajectories. In addition to the above functions, more applications can be achieved with our designer metasurface through appropriate designs.

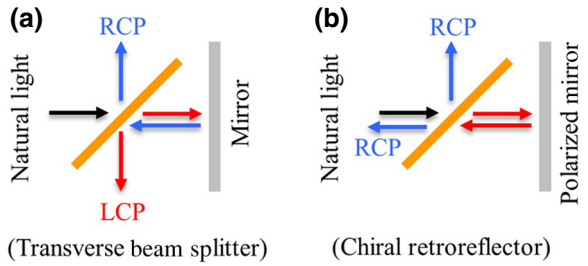

FIG. 6. Applications of the designer photonic heterostructure. (a) Schematic illustration of a transverse beam splitter by combining the heterostructure with an ordinary metallic mirror. Natural light, with randomly polarized photons, can be divided into two transverse trajectories. (b) An example of chiral retroreflector from the combination of the designer heterostructure and a polarized mirror.

III. CONCLUSION

In summary, we achieve a giant spin-flipped chiroptical response by applying the concept of a heterostructure to chiral photonics. All incident photons can be separated into two orthogonal trajectories with the flipped spin states by a flip-stacked metasurface. We apply symmetry group analysis and numerical simulations to reveal the implicit mechanism of interlayer coupling in photonic heterostructures. To verify the theory, a proof-of-concept heterostructure is designed and demonstrated at the microwave region. The simulated and experimented results coincide with the theoretical analysis. Moreover, our designer metasurface proves to be insensitive to the polarization of the incidence. Due to these features, our

design could serve as a good candidate for a chiral beam splitter and many applications can be realized by combining it with other elements. Finally, we expect the methodology of photonic heterostructure might provide an alternative pathway for designing advanced electromagnetic metamaterials.

ACKNOWLEDGMENTS

This work is sponsored by the National Key Research and Development Program of China (Grants No. 2018YFA0209001 and No. 2018YFB2200703), the National Natural Science Foundation of China (Grant No. 61801268), the Natural Science Foundation of Shandong Province (No. ZR2018QF001), the Fundamental Research Funds of Shandong University (No. 2017TB0014), and the Young Scholars Program of Shandong University.

C. Niu and Z. Wang contributed equally to this work.

APPENDIX A

1. Radiation of the hybrid surface polarizations

In this section, we aim to find scattering responses of generic planar intefaces with tangential polarization vectors $\mathbf{P}_{\mathrm{TE}}$ and $\mathbf{M}_{\mathrm{TE}}$. The radiated fields evaluated at the boundary are given by

$$\mathbf{E}^{>}_{t,\mathrm{rad}} = \frac{i\omega}{2}\overline{\overline{Z}}\cdot[\mathbf{P}_{\mathrm{TE}} - \overline{\overline{Z}}^{-1}\cdot\hat{z}\times\mathbf{M}_{\mathrm{TE}}], \tag{A1}$$

$$\mathbf{E}^{<}_{t,\mathrm{rad}} = \frac{i\omega}{2}\overline{\overline{Z}}\cdot[\mathbf{P}_{\mathrm{TE}} + \overline{\overline{Z}}^{-1}\cdot\hat{z}\times\mathbf{M}_{\mathrm{TE}}]. \tag{A2}$$

When the plane of incidence is fixed to the xz plane, the transverse wave vector is $\mathbf{k}_t = \hat{x}k_x$, and the dyadic $\overline{\overline{Z}}$ can be expressed as $\overline{\overline{Z}} = \eta[\hat{x}\hat{x}\cos\theta + \hat{y}\hat{y}(1/\cos\theta)]$. Substituting each tangential components of the polarization ($\mathbf{P}_{\mathrm{TE}} = \hat{x}P^x_{\mathrm{TE}} + \hat{y}P^y_{\mathrm{TE}}$, $\mathbf{M}_{\mathrm{TE}} = \hat{x}M^x_{\mathrm{TE}} + \hat{y}M^y_{\mathrm{TE}}$) into Eqs. (A1) and (A2), we can obtain

$$\mathbf{E}^{>}_{t,\mathrm{rad}} = \frac{i\omega}{2}\left[\hat{x}(\eta P^x_{\mathrm{TE}}\cos\theta + M^y_{\mathrm{TE}}) + \hat{y}\left(\eta P^y_{\mathrm{TE}}\frac{1}{\cos\theta} - M^x_{\mathrm{TE}}\right)\right], \tag{A3}$$

$$\mathbf{E}^{<}_{t,\mathrm{rad}} = \frac{i\omega}{2}\left[\hat{x}(\eta P^x_{\mathrm{TE}}\cos\theta - M^y_{\mathrm{TE}}) + \hat{y}\left(\eta P^y_{\mathrm{TE}}\frac{1}{\cos\theta} + M^x_{\mathrm{TE}}\right)\right]. \tag{A4}$$

To ensure zero reflection under RCP illuminations, the radiated fields from electric and magnetic polarizations must destructively interfere, that is, $\mathbf{E}^{>}_{t,\mathrm{rad}} = 0$. The necessary condition relates the complex amplitudes of the tangential polarizations

$$M^x_{\mathrm{TE}} = \eta P^y_{\mathrm{TE}}\frac{1}{\cos\theta},\ M^y_{\mathrm{TE}} = -\eta P^x_{\mathrm{TE}}\cos\theta. \tag{A5}$$

Meanwhile, the radiated field in the lower space ($\mathbf{E}^{<}_{t,\mathrm{rad}}$) must consist of two parts: a radiated RCP wave to destructively interfere with the incidence ($\mathbf{E}^{i}_{t}$), and a LCP wave with an equal amplitude to produce near-perfect performance of spin flipping. Consequently, the radiated field $\mathbf{E}^{<}_{t,\mathrm{rad}}$ should be pure linear polarization. Hence, another relationship between the tangential polarizations can be given by

$$\frac{P^x_{\mathrm{TE}}}{P^y_{\mathrm{TE}}} = \left(\frac{P^x_{\mathrm{TE}}}{P^y_{\mathrm{TE}}}\right)^*,\ \frac{M^x_{\mathrm{TE}}}{M^y_{\mathrm{TE}}} = \left(\frac{M^x_{\mathrm{TE}}}{M^y_{\mathrm{TE}}}\right)^*, \tag{A6}$$

which means the incident RCP waves can induce x- and y-component polarizations with the same phase profile.

2. Change the linear basis to the circular basis

Assume $\vec{u}$ and $\vec{v}$ are the two linear bases that represent u and v polarizations for an arbitrary port, respectively, and $\vec{\beta}_+$ and $\vec{\beta}_-$ are the two circular bases of RCP and LCP waves, respectively.

(1) Case 1: wave propagates along the $+w$ direction (input modes).

In this case, two circular polarizations can be decomposed into the combinations of two linear polarizations

$$\vec{\beta}^{\mathrm{in}}_{+} = \frac{1}{\sqrt{2}}(\vec{u} + i\vec{v}),\ \vec{\beta}^{\mathrm{in}}_{-} = \frac{1}{\sqrt{2}}(\vec{u} - i\vec{v}). \tag{A7}$$

The transformation matrix $\mathbf{P}$ relates two bases

$$(\vec{\beta}^{\mathrm{in}}_{+}, \vec{\beta}^{\mathrm{in}}_{-})\mathbf{P}^{-1} = (\vec{u}, \vec{v}). \tag{A8}$$

Substituting Eq. (A7) into Eq. (A8), we can obtain the transformation matrix

$$\mathbf{P} = \frac{1}{\sqrt{2}}\begin{bmatrix} 1 & 1 \\ i & -i \end{bmatrix}. \tag{A9}$$

(2) Case 2: wave propagates along the $-w$ direction (output modes).

In this case, because the propagating direction is reversed, we must decompose two circular polarizations

into different combinations

$$\vec{\beta}_+^{\text{out}} = \frac{1}{\sqrt{2}}(-\vec{u} + i\vec{v}),\ \vec{\beta}_-^{\text{out}} = \frac{1}{\sqrt{2}}(-\vec{u} - i\vec{v}). \quad \text{(A10)}$$

Similarly, another transformation matrix, **Q**, relates two bases

$$(\vec{\beta}_+^{\text{out}}, \vec{\beta}_-^{\text{out}})\mathbf{Q}^{-1} = (\vec{u}, \vec{v}). \quad \text{(A11)}$$

Then matrix **Q** can be derived from Eqs. (A10) and (A11)

$$\mathbf{Q} = \frac{1}{\sqrt{2}}\begin{bmatrix} -1 & -1 \\ i & -i \end{bmatrix}. \quad \text{(A12)}$$

3. The scattering matrix for circular polarizations

An arbitrary incident mode from the m-th port can be expressed in the linear basis as

$$\vec{E}_i = x_u\vec{u}_m + x_v\vec{v}_m = (\vec{u}_m, \vec{v}_m)[x_u, x_v]^T, \quad \text{(A13)}$$

or in the circular basis (propagating in the $+w$ direction) as

$$\begin{aligned}\vec{E}_i &= y_+\vec{\beta}_+^{\text{in}} + y_-\vec{\beta}_-^{\text{in}} = (\vec{\beta}_+^{\text{in}}, \vec{\beta}_-^{\text{in}})[y_+, y_-]^T \\ &= (\vec{u}_m, \vec{v}_m)\mathbf{P}[y_+, y_-]^T. \end{aligned} \quad \text{(A14)}$$

The scattered fields going to the n-th port can be written in a similar way, with the linear basis

$$\vec{E}_s = x_u^s\vec{u}_n + x_v^s\vec{v}_n = (\vec{u}_n, \vec{v}_n)[x_u^s, x_v^s]^T, \quad \text{(A15)}$$

and the circular basis

$$\begin{aligned}\vec{E}_s &= y_+^s\vec{\beta}_+^{\text{out}} + y_-^s\vec{\beta}_-^{\text{out}} = (\vec{\beta}_+^{\text{out}}, \vec{\beta}_-^{\text{out}})[y_+^s, y_-^s]^T \\ &= (\vec{u}_n, \vec{v}_n)\mathbf{Q}[y_+^s, y_-^s]^T. \end{aligned} \quad \text{(A16)}$$

The scattering matrix relates the input and output fields and can be expressed in the linear basis

$$[x_u^s, x_v^s]^T = \mathbf{S}_{nm}[x_u, x_v]^T, \quad \text{(A17)}$$

or the circular basis

$$[y_+^s, y_-^s]^T = \mathbf{S}_{\text{circ}}[y_+, y_-]^T. \quad \text{(A18)}$$

Combining Eqs. (A14)–(A18), we can thus obtain the relationship between the matrices

$$\mathbf{S}_{\text{circ}} = \mathbf{Q}^{-1}\mathbf{S}_{nm}\mathbf{P}. \quad \text{(A19)}$$

4. Proof of Eq. (7) that $\mathbf{S}_{\text{circ}}^f = (\mathbf{S}_{\text{circ}}^b)^T$

The scattering matrix, $\mathbf{S}_{nm}$ (for either reflection or transmission), relates how the incident wave from the m-th port scatters into the n-th port. Here, we denote it as the forward scattering matrix and convert it into the circular basis

$$\mathbf{S}_{\text{circ}}^f = \mathbf{Q}^{-1}\mathbf{S}_{nm}\mathbf{P}, \quad \text{(A20)}$$

Similarly, due to the reciprocal property ($\mathbf{S}_{mn} = \mathbf{S}_{nm}^T$), the backward scattering matrix is given by

$$\mathbf{S}_{\text{circ}}^b = \mathbf{Q}^{-1}\mathbf{S}_{mn}\mathbf{P} = \mathbf{Q}^{-1}\mathbf{S}_{nm}^T\mathbf{P}, \quad \text{(A21)}$$

By substituting Eq. (A20) into Eq. (A21), we can prove that $\mathbf{S}_{\text{circ}}^f = (\mathbf{S}_{\text{circ}}^b)^T$.

APPENDIX B: PERFORMANCE DEPENDENCE ON THE STRUCTURAL PARAMETERS

To investigate changes in reflection and transmission of the proposed metasurface, with respect to the structural parameters and the angle of incidence, we have simulated different situations. Figures 7(a) and 7(b) show

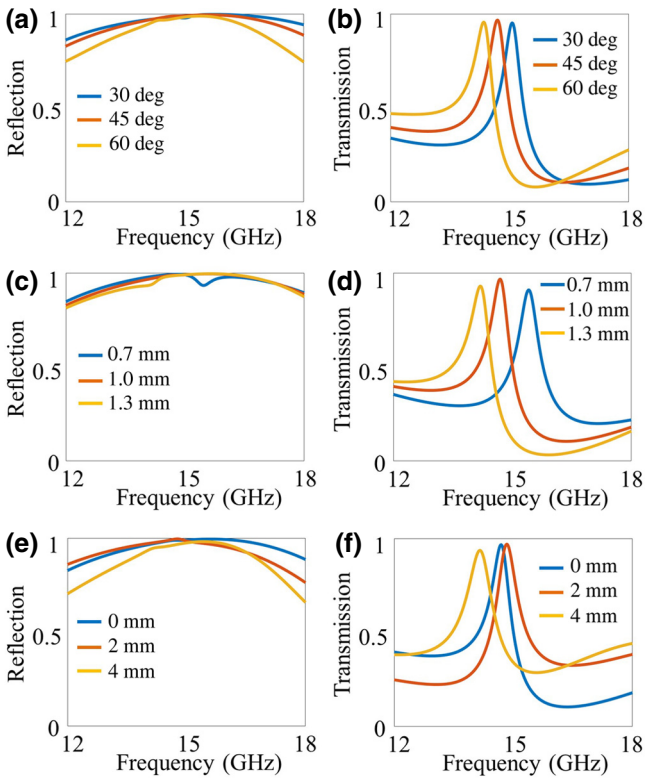

FIG. 7. The dependence of spin-flipped reflection coefficients for LCP and spin-flipped transmission coefficients for RCP on (a),(b) the incident angle, (c),(d) the thickness of the dielectric substrate, and (e),(f) the misalignment between upper and bottom layers along the x direction.

the spin-flipped reflection coefficients for LCP (r_{RL}) and spin-flipped transmission coefficients for RCP (t_{LR}) with incident angles of 30°, 45°, and 60°; substrate thicknesses of 0.7 mm, 1.0 mm, and 1.3 mm; and misalignments between the upper and bottom layers along th e*x* direction of 0 mm, 2 mm, and 4 mm. We see that the amplitude of the coefficients barely changes and the resonant frequency shifts only a little bit; this indicates that a slight change in structural parameters will not significantly affect the performance of the metasurfaces.

[1] L. D. Barron, *Molecular light scattering and optical activity* (Cambridge University Press, New York, 2004).

[2] U. Meierhenrich, *Amino acids and the asymmetry of life: caught in the act of formation* (Springer Science & Business Media, 2008).

[3] R. Naaman and D. H. Waldeck, Chiral-induced spin selectivity effect, J. Phys. Chem. Lett. **3**, 2178 (2012).

[4] R. Naaman and D. H. Waldeck, Spintronics and chirality: Spin selectivity in electron transport through chiral molecules, Annu. Rev. Phys. Chem **66**, 263 (2015).

[5] A. Rodger, B. Nordén, and B. Nordén, *Circular dichroism and linear dichroism* (Oxford University Press, USA, 1997), Vol. 1.

[6] N. Nagaosa and Y. Tokura, Topological properties and dynamics of magnetic skyrmions, Nat. Nanotechnol. **8**, 899 (2013).

[7] A. Fert, N. Reyren, and V. Cros, Magnetic skyrmions: advances in physics and potential applications, Nat. Rev. Mater. **2**, 17031 (2017).

[8] E. Ariens, Stereochemistry, a basis for sophisticated nonsense in pharmacokinetics and clinical pharmacology, Eur. J. Clin. Pharmacol. **26**, 663 (1984).

[9] A. Hutt and S. Tan, Drug chirality and its clinical significance, Drugs **52**, 1 (1996).

[10] Z. Wang, F. Cheng, T. Winsor, and Y. Liu, Optical chiral metamaterials: a review of the fundamentals, fabrication methods and applications, Nanotechnology **27**, 412001 (2016).

[11] M. Hentschel, M. Schäferling, X. Duan, H. Giessen, and N. Liu, Chiral plasmonics, Sci. Adv. **3**, e1602735 (2017).

[12] S. Zhang, Y.-S. Park, J. Li, X. Lu, W. Zhang, and X. Zhang, Negative Refractive Index in Chiral Metamaterials, Phys. Rev. Lett. **102**, 023901 (2009).

[13] Z. Wang, L. Jing, K. Yao, Y. Yang, B. Zheng, C. M. Soukoulis, H. Chen, and Y. Liu, Origami-based reconfigurable metamaterials for tunable chirality, Adv. Mater. **29**, 1700412 (2017).

[14] J. K. Gansel, M. Thiel, M. S. Rill, M. Decker, K. Bade, V. Saile, G. von Freymann, S. Linden, and M. Wegener, Gold helix photonic metamaterial as broadband circular polarizer, Science **325**, 1513 (2009).

[15] A. G. Mark, J. G. Gibbs, T.-C. Lee, and P. Fischer, Hybrid nanocolloids with programmed three-dimensional shape and material composition, Nat. Mater. **12**, 802 (2013).

[16] M. Esposito, V. Tasco, F. Todisco, M. Cuscunà, A. Benedetti, D. Sanvitto, and A. Passaseo, Triple-helical nanowires by tomographic rotatory growth for chiral photonics, Nat. Commun. **6**, 6484 (2015).

[17] A. Kuzyk, R. Schreiber, Z. Fan, G. Pardatscher, E.-M. Roller, A. Hogele, F. C. Simmel, A. O. Govorov, and T. Liedl, DNA-based self-assembly of chiral plasmonic nanostructures with tailored optical response, Nature **483**, 311 (2012).

[18] X. Shen, C. Song, J. Wang, D. Shi, Z. Wang, N. Liu, and B. Ding, Rolling up gold nanoparticle-dressed DNA origami into three-dimensional plasmonic chiral nanostructures, J. Am. Chem. Soc. **134**, 146 (2012).

[19] N. Liu, H. Liu, S. Zhu, and H. Giessen. Stereometamaterials, Nat. Photon. **3**, 157 (2009).

[20] Y. Zhao, M. Belkin, and A. Alù, Twisted optical metamaterials for planarized ultrathin broadband circular polarizers, Nat. Commun. **3**, 870 (2012).

[21] Y. Cui, L. Kang, S. Lan, S. Rodrigues, and W. Cai, Giant chiral optical response from a twisted-arc metamaterial, Nano Lett. **14**, 1021 (2014).

[22] L. Kang, S. Lan, Y. Cui, S. P. Rodrigues, Y. Liu, D. H. Werner, and W. Cai, An active metamaterial platform for chiral responsive optoelectronics, Adv. Mater. **27**, 4377 (2015).

[23] M. Hentschel, M. Schäferling, B. Metzger, and H. Giessen, Plasmonic diastereomers: adding up chiral centers, Nano Lett. **13**, 600 (2013).

[24] Z. Wu and Y. Zheng, Moiré chiral metamaterials, Adv. Opt. Mater. **5**, 1700034 (2017).

[25] X. Yin, M. Schaeferling, B. Metzger, and H. Giessen, Interpreting chiral nanophotonic spectra: the plasmonic Born-Kuhn model, Nano Lett. **13**, 6238 (2013).

[26] N. Yu and F. Capasso, Flat optics with designer metasurfaces, Nat. Mater. **13**, 139 (2014).

[27] H.-T. Chen, A. J. Taylor, and N. Yu, A review of metasurfaces: physics and applications, Rep. Prog. Phys. **79**, 076401 (2016).

[28] P. Genevet, F. Capasso, F. Aieta, M. Khorasaninejad, and R. Devlin, Recent advances in planar optics: from plasmonic to dielectric metasurfaces, Optica **4**, 139 (2017).

[29] S. B. Glybovski, S. A. Tretyakov, P. A. Belov, Y. S. Kivshar, and C. R. Simovski, Metasurfaces: From microwaves to visible, Phys. Rep. **634**, 1 (2016).

[30] A. Papakostas, A. Potts, D. Bagnall, S. Prosvirnin, H. Coles, and N. Zheludev, Optical Manifestations of Planar Chirality, Phys. Rev. Lett. **90**, 107404 (2003).

[31] M. Kuwata-Gonokami, N. Saito, Y. Ino, M. Kauranen, K. Jefimovs, T. Vallius, J. Turunen, and Y. Svirko, Giant Optical Activity in Quasi-Two-Dimensional Planar Nanostructures, Phys. Rev. Lett. **95**, 227401 (2005).

[32] A. Y. Zhu, W. T. Chen, A. Zaidi, Y.-W. Huang, M. Khorasaninejad, V. Sanjeev, C.-W. Qiu, and F. Capasso, Giant intrinsic chiro-optical activity in planar dielectric nanostructures, Light Sci. Appl. **7**, 17158 (2018).

[33] A. S. Karimullah, C. Jack, R. Tullius, V. M. Rotello, G. Cooke, N. Gadegaard, L. D. Barron, and M. Kadodwala, Disposable plasmonics: Plastic templated plasmonic metamaterials with tunable chirality, Adv. Mater. **27**, 5610 (2015).

[34] W. Ye, X. Yuan, C. Guo, J. Zhang, B. Yang, and S. Zhang, Large Chiroptical Effects in Planar Chiral Metamaterials, Phys. Rev. Appl. **7**, 054003 (2017).

[35] V. K. Valev, J. J. Baumberg, C. Sibilia, and T. Verbiest, Chirality and chiroptical effects in plasmonic nanostructures: fundamentals, recent progress, and outlook, Adv. Mater. **25**, 2517 (2013).

[36] D. Jalas, A. Y. Petrov, M. Eich, W. Freude, S. Fan, Z. Yu, R. Baets, M. A. Popovic, A. Melloni, and J. D. Joannopoulos, What is—and what is not—an optical isolator, Nat. Photon. **7**, 579 (2013).

[37] R. J. Potton, Reciprocity in optics, Rep. Prog. Phys. **67**, 717 (2004).

[38] E. Plum, X. X. Liu, V. A. Fedotov, Y. Chen, D. P. Tsai, and N. I. Zheludev, Metamaterials: Optical Activity without Chirality, Phys. Rev. Lett. **102**, 113902 (2009).

[39] E. Plum, V. A. Fedotov, and N. I. Zheludev, Specular optical activity of achiral metasurfaces, Appl. Phys. Lett. **108**, 141905 (2016).

[40] M. Albooyeh, D.-H. Kwon, F. Capolino, and S. Tretyakov, Equivalent realizations of reciprocal metasurfaces: Role of tangential and normal polarization, Phys. Rev. B **95**, 115435 (2017).

[41] Y. Ra'di, C. R. Simovski, and S. A. Tretyakov, Thin Perfect Absorbers for Electromagnetic Waves: Theory, Design, and Realizations, Phys. Rev. Appl. **3**, 037001 (2015).

[42] W. Suh, Z. Wang, and S. Fan, Temporal coupled-mode theory and the presence of non-orthogonal modes in lossless multimode cavities, IEEE J. Quantum Electron. **40**, 1511 (2004).

[43] S. S. Kruk, A. N. Poddubny, D. A. Powell, C. Helgert, M. Decker, T. Pertsch, D. N. Neshev, and Y. S. Kivshar, Polarization properties of optical metasurfaces of different symmetries, Phys. Rev. B **91**, 195401 (2015).

[44] C. Rizza, A. Di Falco, M. Scalora, and A. Ciattoni, One-Dimensional Chirality: Strong Optical Activity in Epsilon-Near-Zero Metamaterials, Phys. Rev. Lett. **115**, 057401 (2015).

[45] L. Arnaut, Chirality in multi-dimensional space with application to electromagnetic characterisation of multi-dimensional chiral and semi-chiral media, J. Electromagn. Waves. Appl. **11**, 1459 (1997).

[46] A. Ciattoni and C. Rizza, Nonlocal homogenization theory in metamaterials: Effective electromagnetic spatial dispersion and artificial chirality, Phys. Rev. B **91**, 184207 (2015).

[47] Z. Wang, K. Yao, M. Chen, H. Chen, and Y. Liu, Manipulating Smith-Purcell Emission with Babinet Metasurfaces, Phys. Rev. Lett. **117**, 157401 (2016).

[48] P. C. Wu, W. Y. Tsai, W. T. Chen, Y. W. Huang, T. Y. Chen, J. W. Chen, C. Y. Liao, C. H. Chu, G. Sun, and D. P. Tsai, Versatile polarization generation with an aluminum plasmonic metasurface, Nano Lett. **17**, 445 (2017).

[49] M. Khorasaninejad and K. B. Crozier, Silicon nanofin grating as a miniature chirality-distinguishing beam-splitter, Nat. Commun. **5**, 5386 (2014).

[50] G. X. Zheng, H. Muhlenbernd, M. Kenney, G. X. Li, T. Zentgraf, and S. Zhang, Metasurface holograms reaching 80% efficiency, Nat. Nanotechnol. **10**, 308 (2015).

[51] V. A. Fedotov, P. L. Mladyonov, S. L. Prosvirnin, A. V. Rogacheva, Y. Chen, and N. I. Zheludev, Asymmetric Propagation of Electromagnetic Waves through a Planar Chiral Structure, Phys. Rev. Lett. **97**, 167401 (2006).

[52] C. Menzel, C. Helgert, C. Rockstuhl, E. B. Kley, A. Tünnermann, T. Pertsch, and F. Lederer, Asymmetric Transmission of Linearly Polarized Light at Optical Metamaterials, Phys. Rev. Lett. **104**, 253902 (2010).

[53] C. Rizza, X. Li, A. Di Falco, E. Palange, A. Marini, and A. Ciattoni, Enhanced asymmetric transmission in hyperbolic epsilon-near-zero slabs, J. Opt. **20**, 085001 (2018).

[54] Z. Wang, H. Jia, K. Yao, W. Cai, H. Chen, and Y. Liu, Circular dichroism metamirrors with near-perfect extinction, ACS Photonics. **3**, 2096 (2016).